Polym. Bull. (2016) 73:1761–1773
DOI 10.1007/s00289-015-1575-1

ORIGINAL PAPER

CdSe tetrapods-modified ZnO cathode buffer layers for enhancement of power conversion efficiency in inverted polymer solar cells

Licheng Tan[1] · Cong Liu[1] · Haiyan Fu[1] · Yan Zhang[1]

Received: 13 August 2015 / Revised: 21 September 2015 / Accepted: 18 November 2015 /
Published online: 27 November 2015

Abstract CdSe tetrapods (TPs)-modified ZnO served as cathode buffer layer in the inverted polymer solar cell, could not only passivate the surface defects of ZnO, but also fabricate electron percolation pathways and reduce the band offset at the interface between cathode and active layer, which could promote effective carrier transfer and reduce the rate of surface recombination, and thus boost the device efficiency. The improved crystal quality of ZnO and photon absorption are in favor of the increasing of the short-circuit current density (J_{sc}). The decreased series resistance (R_s) and increased shunt resistance (R_{sh}) of the entire devices, are beneficial to the fill factor (FF) enhancement. By optimizing the content of CdSe TPs, the power conversion efficiency of the inverted device based on ZnO/CdSe-2 has been greatly improved to 2.91 % with high J_{sc} of 8.03 mA/cm^2 and FF of 61.3 %.

Graphical abstract

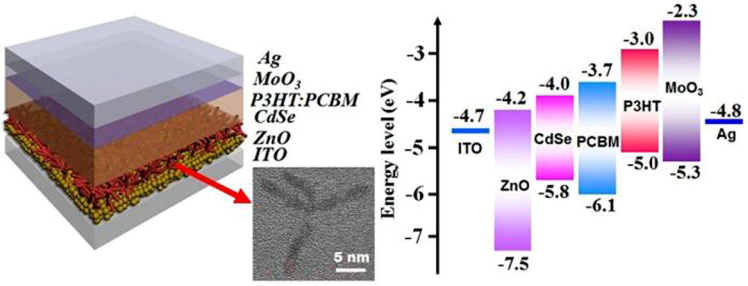

✉ Licheng Tan
tanlicheng@ncu.edu.cn

[1] Institute of Polymers/College of Chemistry, Nanchang University, 999 Xuefu Avenue, Nanchang 330031, China

Keywords CdSe tetrapods · Cathode buffer layers · ZnO · Nanocrystals · Inverted polymer solar cells

Introduction

Great attention has been attracted by organic photovoltaics (OPVs), which becoming a promising candidate for future energy sources due to their low cost, high performance, and mechanically flexible properties and reached 10 % for the conventional devices (substrate/hole transporting/active layer/electron transporting) [1]. Typically, the conventional device structure is sandwiched by poly(3, 4-ethylenedioxylenethiophene):polystyrene sulfonic acid (PEDOT:PSS) on the indium tin oxide (ITO) glasses as the anode and the low work function metal, such as Al, as the cathode [2]. However, PEDOT:PSS has several problems including high acidity, hygroscopic property and inhomogeneous electrical property, resulting in poor long-term stability, and thus degrades the OPV performance rapidly [3]. Accordingly, an inverted device structure has been adopted to alleviate this stability problem [4]. Moreover, the ideal process for inverted solar cell fabrication would be to use solution-processing techniques to deposit the different layers in the solar cell and is thus more compatible with roll-to-roll manufacturing processes than that for the conventional cells. In the inverted structure, the carrier collection nature of the electrodes is reversed, with a high work function metal (such as Au and Ag) as the anode and the ITO electrode as the cathode [5]. As compared to the conventional ones, inverted device architectures tend to exhibit low fill factor (FF) and photocurrent, leading to unsatisfactory conversion efficiency [6].

For resolving the issue of low FF and photocurrent in the inverted solar cells, much effort has been focused on the optimization of morphologies and electronic structures of active materials by developing advanced processing methods for superior optical absorption and charge separation, improving the interface between contact electrodes and active materials, and understanding underlying device physics [7]. One of the major focuses is to use some of the buffer (or interfacial) layers to modify the ITO interface to decrease the work function for efficiently collecting electrons since the work function of ITO is usually not aligned with the lowest unoccupied molecular orbital (LUMO) of fullerenes [8]. The most popular n-type buffer layers are TiO_2 and ZnO, which enable the unipolar extraction of photo generated electrons from the active layers to the ITO electrodes [9]. Even though reasonable efficiencies have been reached with TiO_2 and ZnO buffer layers in the inverted solar cells, the development of interfacial engineering is being intensely pursued [10]. Self-assembled monolayer-modified ZnO/metals as cathodes show dramatic improvements in power conversion efficiency (PCE) [11]. These approaches could be beneficial for the future development of printable solar cells [12]. Moreover, it has been shown that the power conversion efficiencies of these devices depend on establishing a percolation network as interfacial layer for electrons extraction and regulating the shape of the nanoparticles in the interfacial layer [13]. For example, devices with nanorods as interfacial layer show better

efficiencies than those based on spherical nanoparticles because of existing fewer interparticle hops which hinder the electrons extraction from the active layer [14]. Furthermore, three-dimensional (3D) branched structures of metal oxide have been demonstrated to be another approach to improve the PCE due to the increased interface of the acceptor/buffer layer and formed electron percolation pathways perpendicular to the substrate, which improves the electron transport and is expected to allow for thicker active layers [15].

In general, devices where spherical particles are replaced by nanorods show better efficiencies because of providing the ability of extracting electrons due to fewer interparticle hops. Additionally, forming electron percolation pathways perpendicular to the substrate by employing 3D branched nanocrystals, the photovoltaic efficiency can further be improved. In this work, spin-coated sol–gel ZnO nanoparticles modified with CdSe tetrapods (TPs) have been served as an effective buffer layer for OPVs based on poly(3-hexylthiophene):(6,6)-phenyl-C61-butyric acid methylester (P3HT:PCBM). The addition of CdSe TPs is able to suppress carrier recombination and increase electron collection efficiency via: (a) improving the crystal quality of ZnO, (b) increasing the photon absorption, and (c) a better energy level alignment at the organic/cathode interface by lowering the work function of ZnO. By modifying sol–gel ZnO buffer layers with optimum CdSe TPs, the OPV devices with P3HT:PCBM exhibit improved short-circuit current density (J_{sc}) from 7.39 mA cm^{-2} to 8.03 mA cm^{-2}, fill factor (FF) from 52.9 to 61.3 %, as thus achieves the enhancement of PCE to 2.91 %.

Experimental

Materials

Cadmium oxide (CdO), oleic acid (OA), 1-octadecene (ODE) and o-dichlorobenzene(o-DCB, spectrum pure) were purchased from Alfa Aesar and used as received without any further purification. And other chemicals were obtained from Shanghai Reagent Co., Ltd. and used as received. Regioregular P3HT (Mw = 48,300 g/mol, head-to-tail, regioregularity >90 %), [6,6]-phenyl-C61-butyric acid methyl ester (PCBM) (99.5 % purity) were purchased from Rieke Metals, Inc. and Nano-C. Indium tin oxide (ITO) glass was obtained from Delta Technologies Limited.

Synthesis of CdSe TPs

Cadmium oxide (CdO, 1 mmol), oleic acid (OA, 6 mmol) and 20 mL 1-octadecene (ODE) were pumped at 140 °C under a N_2 flow for 30 min. After that, the temperature was first raised to about 240 °C. When solution turned clear, the temperature is decreased to 190 °C, then CTAB-hexadecyl trimethyl ammonium bromide (TOP-Se-CTAB) solution (containing 1 mL TOP, 0.5 mmol Se, 0.05 mmol CTAB and 3 mL toluene) was quickly injected. The injection caused a temperature drop to about 165 °C, where the reaction occurred and persisted for 1 h to grow CdSe TPs. And then, the heating mantle was removed, and the solution

was cooled to room temperature. Afterwards, 10 mL acetone was injected to collect the red precipitation followed by centrifugation at 4500 rpm. The obtained CdSe TPs were cleaned with chlorobenzene/acetone solvent/antisolvent at least six times and then dissolved in chlorobenzene to form a clear red solution with a desired concentration.

Fabrication solar cells

After cleaning the ITO-coated glass substrate, the sol–gel ZnO was spin-coated four times (10 s each time) with a spin-coater at 4000 rpm to yield a 100 nm-thick film. The deposited films were thermally treated at 200 °C for 10 min in each deposition. CdSe TPs with 8 mg/mL, 5 mg/mL and 3 mg/mL, named as ZnO/CdSe-1, ZnO/CdSe-2, ZnO/CdSe-3, respectively, were spin-coated on the ZnO layer for one time. The samples were then annealed in air for 0.5 h at 250 °C. P3HT (15 mg, purchased from Rieke Metals, used as received) and $PC_{61}BM$ (15 mg, purchased from Nano-C, used as received) were dissolved in 1 mL 1,2-dichlorobenzene (DCB) to obtain P3HT:$PC_{61}BM$ (1:1 w/w) solution. Then P3HT:PCBM solution was spin-coated on top of the CdSe TPs layer at 800 rpm in glove box and dried in covered glass Petri dish (solvent annealing). The fabrication of the solar cells was finished by the evaporation of 6 nm MoO_3 followed by 100 nm Ag on top. A shadow mask was used to define six separated devices, each with a diameter of 2 mm.

Characterization

The structure of CdSe TPs was characterized by transmission electron microscopy (TEM, FEI E.O Tecnai F20 G2 MAT S-TWIN). Atomic Force Microscope (AFM) images were observed with Digital Instrumental Nanoscope 31. The Raman spectra of pristine ZnO and after modification by CdSe TPs were measured with a resolution of about 1.2 cm^{-1} and the analysis range among 100–1000 cm^{-1}. Optical absorptions of the CdSe TPs were measured using a UV–vis-IR spectrophotometer (JASCO V-670). X-ray diffraction (XRD) study of the samples was carried out on a Bruker D8 Focus X-ray diffractometer operating at 30 kV and 20 mA with a copper target ($\lambda = 1.54$ Å) and at a scanning rate of 1°/min. X-ray photoelectron spectroscopy (XPS) studies were performed on a thermo-VG scientific ESCALAB 250 photoelectron spectrometer using a monochromated AlKa (1486.6 eV) X-ray source. The work function was investigated by ultraviolet photoelectron spectroscopy (UPS) using Thermo-VG Scientific ESCALAB 250 with a He I (21.22 eV) discharge lamp. A bias of −8.0 V was applied to the samples for separation of the sample and the secondary edge for the analyzer. Current–voltage (*J*–*V*) characteristics were recorded using a Keithley 2400 Source Meter in the dark and under 100 mW cm^2 simulated AM 1.5 G irradiation (Abet Solar Simulator Sun 2000). All the measurements were performed under ambient atmosphere at room temperature.

Results and discussion

Figure 1 shows transmission electron micrograph (TEM) images of branched nanoparticles deposited on a carbon film. A large fraction of branched nanoparticles has been obtained with the shape like tetrapod. Therefore, the branched nanoparticles are referred as "tetrapods", accordingly abbreviating to "TPs". The tetrapod limbs are typically 10–15 nm long and 2 nm thick, corresponding to an approximately total height of 20 nm. CdSe TPs show a good dispersion in organic solvent with weak polarity (such as chlorobenzene, toluene, ODE, OA), making it possible for the deposition on the ZnO layer. High resolution TEM (HRTEM) image shows the crystallized CdSe TPs with the interplanar distances of about 0.35 nm. [16].

Atomic force microscopy (AFM) analysis of different cathode buffer layers (CBLs) has also been investigated in Fig. 2. The complex was spin-coated on ITO substrate, then ZnO and CdSe TPs were annealed at 200 °C at 140 °C, respectively. The thicknesses of ZnO film are approximately 30–40 nm. The pristine ZnO provide a smooth film (RMS = 1.48 nm). As CdSe TPs spin-coated on the ZnO films with 8 mg/mL, the smoothness of the whole layer become worse suddenly

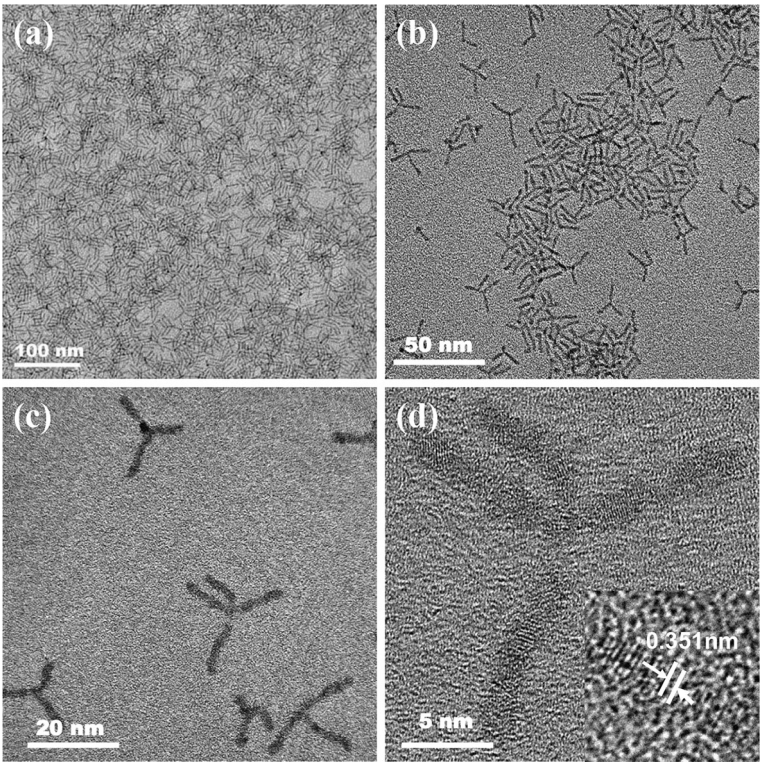

Fig. 1 **a**, **b**, **c** TEM images of CdSe TPs with different scales and **d** high resolution TEM (HRTEM) images

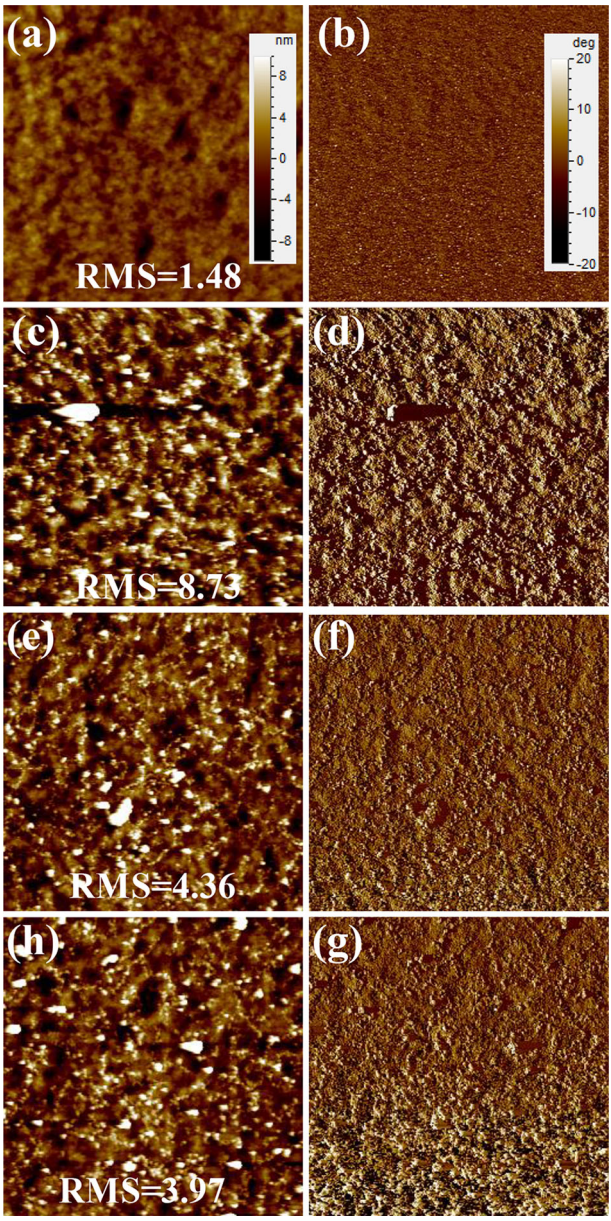

Fig. 2 Atomic force microscope (AFM) topography and phase images (3 × 3 μm) of **a**, **b** pristine ZnO, **c**, **d** ZnO/CdSe-1, **e**, **f** ZnO/CdSe-2 and **g**, **h** ZnO/CdSe-3, respectively

(RMS = 8.37 nm). This phenomenon can be interpreted that unique branched nanostructure from CdSe makes films more uneven. However, the roughness obviously decreases as the reduction of CdSe amount. ZnO/CdSe-2 and ZnO/CdSe-3 films show the surface roughness of 4.36 nm and 3.97 nm, respectively, which

indicates that CdSe TPs have been homogeneously coated on the surface of ZnO layer. Furthermore, the relative larger roughness will cause more obvious invasion between the active layer and CdSe TPs, which may be good for transporting electrons. But, ZnO/CdSe-1 with too high roughness is not good for the film-formation of active layer. The suitable roughness for ZnO/CdSe-2 leads to the photovoltaic parameters with higher fill factor and short-circuit current density than those of ZnO/CdSe-1 and ZnO/CdSe-3.

Figure 3a shows the absorption spectrum of pyridine-treated CdSe TPs spin-coated on the ITO substrate dissolved in chloroform solution after annealing. The first exciton absorption peak and higher order features indicate low polydispersity and good homogeneity of the size and shape of the nanoparticles, due to weaker quantum confinement, which has also been confirmed by TEM. Figure 3b shows the X-ray diffraction (XRD) spectra of ZnO with and without modification by CdSe TPs. Strong peaks located around 35.4° is correspond to the diffraction from (002) plane of ZnO. According to the full width at half maximum intensity change in the peak at 35.4°, it is shown that ZnO after CdSe TPs modification exhibits larger grain size, implying that CdSe TPs play a role in the grain growth during the annealing process [17]. As shown in Fig. 3c, the Raman signals shows LO1 and LO2 modes of CdSe TPs located at 210 and 420 cm^{-1}. It is noted that there are neither Cd–O nor Zn-Se bond signals in the Raman spectrum, which indicates that the crystalline of CdSe TPs is not affected during the deposition process on ZnO surface. [18].

X-ray photoelectron spectroscopy (XPS) characterization for the entire range of binding energies of the atomic core levels of ZnO and ZnO/CdSe has been applied to evaluate the overall composition and defect repair of ZnO/CdSe. As shown in Fig. 4, the O1s XPS spectra of ZnO and ZnO/CdSe with different CdSe TPs content demonstrate two peaks with non-symmetrical line shape. One peak with lower binding energy (530.1 eV) is assigned to O atoms in ZnO structure, and the other peak with higher binding energy at 531.7 eV corresponds to an oxygen-deficiency component, such as O1s in $Zn(OH)_2$, or the oxygen species adsorbed by the surface hydroxyl groups [19, 20]. The intensity of the peak at 531.7 eV for all ZnO/CdSe samples decreases. This phenomenon is obvious with the increasing content of the CdSe TPs, indicating that the modification of ZnO by in situ growth of CdSe TPs avails to reduce the oxygen-deficient component and increase the number of Zn–O bonds. Therefore, the recombination of electron–hole pairs is reduced, which is beneficial for the performance of devices.

Figure 5 shows the device structure and the energy level diagram of the components of the inverted polymer solar cell based on P3HT:PCBM as active layer and pristine ZnO and modified ZnO as cathode buffer layer, respectively. CdSe TPs were dispersed at ZnO buffer layers before depositing P3HT:PCBM. Calculated form the ultraviolet photoelectron spectroscopy (UPS), the conduction band minimum (CBM) of CdSe TPs (−4.0 eV) lies between the LUMO of PCBM (−3.7 eV) and the CBM of ZnO (−4.2 eV), which creating a cascade band structure from PCBM to ZnO. The decrease in band offset at the interface between cathode and active layer could facilitate effective carrier transfer and reduce the rate of surface recombination, and thus enhancing the carrier collection efficiency [21].

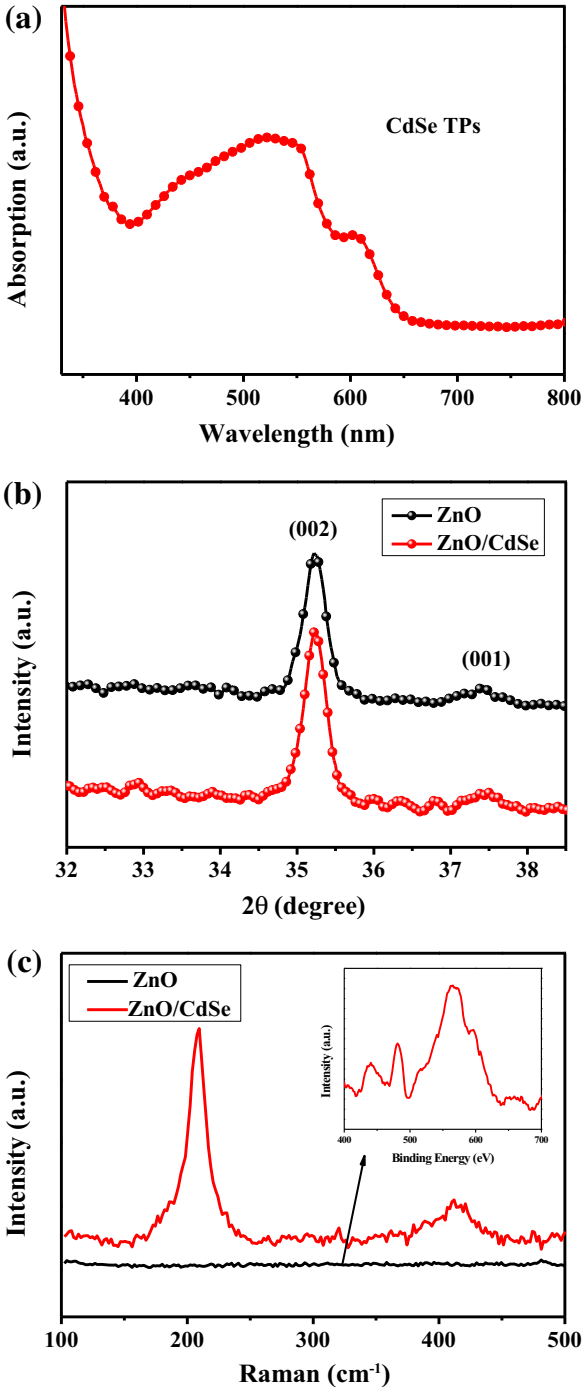

Fig. 3 **a** UV–visible absorption spectrum of CdSe TPs, **b** X-ray diffraction (XRD) and **c** Raman signals of ZnO before and after modification by CdSe TPs

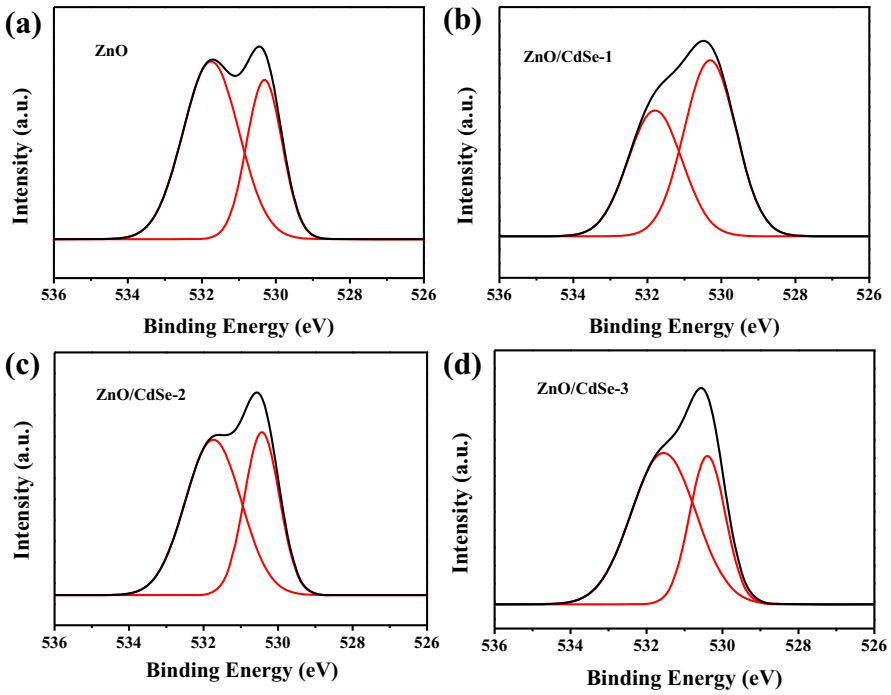

Fig. 4 X-ray photoelectron spectroscopy (XPS) spectra for the O1s of ZnO/CdSe with various content of CdSe TPs

The electron transport characteristics have been measured by the space charge limited current (SCLC) of pristine ZnO and ZnO/CdSe, and the corresponding electron-only devices with ITO/ZnO or (ZnO/CdSe)/P3HT:PCBM/LiF/Al are presented in Fig. 6. It shows $J^{0.5}$–V characteristics plotted for Mot-Gurney SCLC fitting of electron-only devices at ambient temperature. The holes can be effectively blocked due to the mismatched energy levels of the valence band of ZnO and the work function of Al in these devices. The electron mobility can be characterized:

$$J = 9\varepsilon_0\varepsilon_r\mu V^2/8L^3$$

where J is the current density, ε_0 is the dielectric constant of free space, ε_r is the permittivity of the active layer, μ is the electron mobility, V is the internal voltage in the device and L is the thickness of the active layer. As presented in Table 1, the electron mobility for pristine ZnO is only 2.20×10^{-4} cm^2 V^{-1} s^{-1}, while that of ZnO/CdSe-2 is remarkably enhanced to 3.80×10^{-4} cm^2 V^{-1} s^{-1}. The electron mobility of ZnO/CdSe-1 and ZnO/CdSe-3 are 3.45×10^{-4} $cm^2 \cdot V^{-1}$ s^{-1} and 3.13×10^{-4} $cm^2 \cdot V^{-1}$ s^{-1}, respectively, which are lower than that of ZnO/CdSe-2.

Figure 7 shows the steady-state J–V characteristics of devices based on pristine ZnO, ZnO/CdSe TPs with different contents as cathode buffer layer under AM 1.5G illumination, and the corresponding photovoltaic performance are summarized in Table 2. With the addition of CdSe TPs, the short-circuit current density (J_{sc}), fill

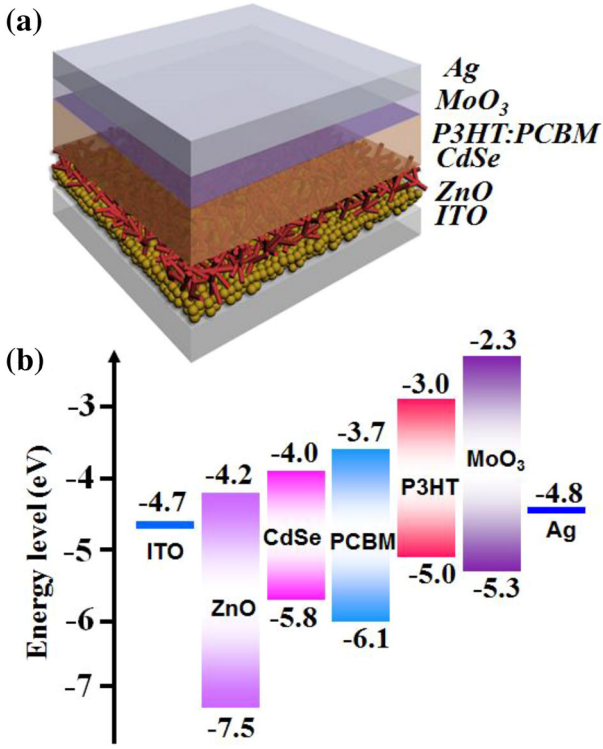

Fig. 5 **a** Device structure and **b** energy level diagram of the components of the devices based on P3HT:PCBM and modified ZnO by CdSe TPs

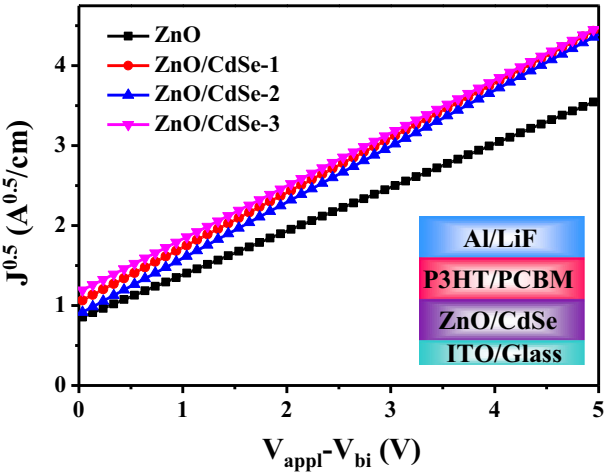

Fig. 6 $J^{0.5}$–V characteristics of electron-only with different cathode buffer layers (CBLs) based on the structure ITO/CBLs/P3HT:PCBM/LiF/Al

Table 1 Summary of the electron mobility of the P3HT:PCBM device with various cathode buffer layers (CBLs)

Device	ZnO	ZnO/CdSe-1	ZnO/CdSe-2	ZnO/CdSe-3
μ (cm^2 V^{-1} s^{-1})	2.20×10^{-4}	3.45×10^{-4}	3.80×10^{-4}	3.13×10^{-4}

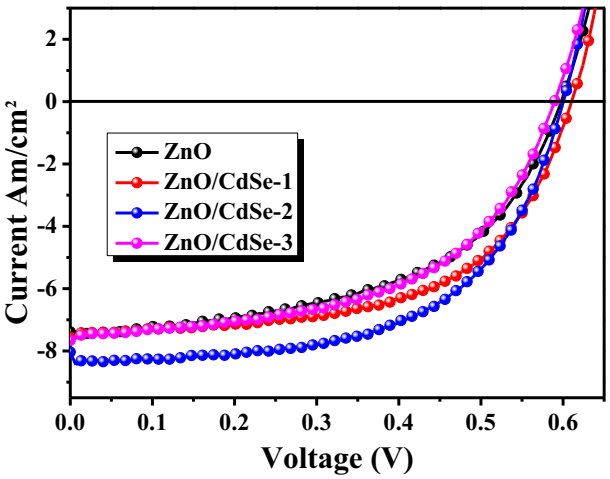

Fig. 7 *J–V* characteristics of the photovoltaic devices with different cathode buffer layers (CBLs) under AM 1.5G illumination

Table 2 Photovoltaic parameters of the inverted polymer solar cells based on ZnO and ZnO/CdSe as cathode buffer layer under AM 1.5G illumination

Device	J_{sc} (mA cm^{-2})	V_{oc} (V)	FF (%)	R_s (Ω cm^2)	R_{sh} (Ω cm^2)	PCE (%)
ZnO	7.39	0.597	52.9	3.73	377.6	2.31
ZnO/CdSe-1	7.56	0.605	57.2	2.42	407.5	2.63
ZnO/CdSe-2	8.03	0.597	61.3	1.60	907.2	2.91
ZnO/CdSe-3	7.66	0.594	53.4	2.75	471.2	2.42

factor (FF) and power conversation efficiency (PCE) of devices with ZnO/CdSe are higher than that based on pristine ZnO. The device based on ZnO/CdSe-2 shows the highest PCE of 2.91 %, J_{sc} of 8.03 mA/cm^2 and FF of 61.3 %. The enhancement of FF is mainly affected by the relatively lower series resistance (R_s) and the relatively higher shunt resistance (R_{sh}) with comparison to that based on ZnO, which could suppress the capture of charge and increase the electron transfer rate [22]. The formation of electron percolation pathways for CdSe TPs enhances the electron transport. Moreover, the improved crystal quality of ZnO and photon absorption are in favor of the increasing of J_{sc}.

Conclusions

CdSe TPs nanocrystals have been developed to modify ZnO as cathode buffer layer (CBL) for boosting the photovoltaic performance of the inverted polymer solar cells based on P3HT:PCBM. The modification of ZnO by CdSe TPs avails to improve the crystal quality of ZnO and photon absorption, which are in favor of the increasing of short-circuit current density (J_{sc}). The conduction band minimum (CBM) of CdSe TPs (−4.0 eV) lies between the LUMO of PCBM (−3.7 eV) and the CBM of ZnO (−4.2 eV), which creating a cascade band structure from PCBM to ZnO. The decrease in band offset at the interface between cathode and active layer, as well as the formation of 3D network structural electron transmission and extraction channels facilitate effective carrier transfer and electron–hole recombination suppression, consequently decreasing the series resistance (R_s) and enhancing shunt resistance (R_{sh}) of the entire devices, which is beneficial to the enhancement of fill factor (FF). With comparison to the device based on pristine ZnO as CBL, the device based on ZnO/CdSe-2 shows the highest power conversion efficiency (PCE) of 2.91 %, J_{sc} of 8.03 mA/cm^2 and FF of 61.3 %.

Acknowledgments The financial supports for this work are provided by the National Science Foundation of China (51302130), Natural Science Foundation of Jiangxi Province (20151BAB213013) and Doctoral Programs Foundation of Ministry of Education of China (Grants 20133601120006).

References

1. Kim JY, Lee K, Coates NE, Moses D, Nguyen TQ, Dante M, Heeger AJ (2007) Efficient tandem polymer solar cells fabricated by all-solution processing. Science 317:222–225
2. Tsega M, Kuo DH (2012) Defects and its effects on properties of Cu-deficient $Cu_2ZnSnSe_4$ bulks with different Zn/Sn ratios. Appl Phys Express 5:091201
3. Jørgensen M, Norrman K, Gevorgyan SA, Tromholt T, Andreasen B, Krebs FC (2012) Stability of polymer solar cells. Adv Mater 24:580–612
4. Pawar SM, Pawara BS, Moholkara AV, Choi DS, Yun JH, Moon JH, Kolekar SS, Kim JH (2010) Single step electrosynthesis of Cu_2ZnSnS_4 (CZTS) thin 150 films for solar cell application. Electrochim Acta 55:4057–4061
5. Katagiri H, Jimbo K, Maw WS, Oishi K, Yamazaki M, Araki H, Takeuchi A (2009) Development of CZTS-based thin film solar cells. Thin Solid Films 517:2455–2460
6. Lee K, Kim JY, Park SH, Kim SH, Cho S, Heeger AJ (2007) Stable polymer electronic devices. Adv Mater 19:2445–2449
7. Kippelen B, Brédas JL (2009) Organic photovoltaics. Energy Environ Sci 2:251–261
8. King RR, Law DC, Edmondson KM, Fetzer CM, Kinsey GS, Yoon H, Sherif RA, Karam NH (2007) 40% efficient metamorphic GaInP/GaInAs/Ge multijunction solar cells. Appl Phys Lett 90:183516
9. Su BQ, Greenham NC (2006) Improved efficiency of photovoltaics based on CdSe nanorods and poly (3-hexylthiophene) nanofibers. Phys Chem Chem Phys 8:3557–3560
10. Scher EC, Manna L, Alivisatos AP (2003) Shape control and applications of nanocrystals. Phil Trans R Soc Lond A 361:241–257
11. Liang ZQ, Zhang QF, Wiranwetchayan O, Xi JT, Yang Z, Park K, Li CD, Cao GZ (2012) Effects of the morphology of a ZnO buffer layer on the photovoltaic performance of inverted polymer solar cells. Adv Funct Mater 22:2194–2201
12. Zhang Q, Yodyingyong S, Xi J, Myers D, Cao G (2012) Oxide nanowires for solar cell applications. Nanoscale 4:1436–1445
13. Shin KS, Jo H, Shin HJ, Choi WM, Choi JY, Kim SW (2012) High quality graphene-semiconducting oxide heterostructure for inverted organic photovoltaics. J Mater Chem 22:13032–13038

14. Lightcap IV, Kamat PV (2012) Fortification of CdSe quantum dots with graphene oxide. Excited state interactions and light energy conversion. J Am Chem Soc 134:71097116
15. Grado-Caffaro MA, Grado-Caffaro M (2015) The shift in the optical band-gap of cadmium oxide as chemical potential minus optical potential. Chem Phys Lett 623:72–75
16. Tan FR, Qu SC, Wang L, Jiang QW, Zhang WF, Wang ZG (2014) Core/shell-shaped CdSe/PbS nanotetrapods for efficient organic–inorganic hybrid solar cells. J Mater Chem A 2:14502–14510
17. Woldu T, Raneesh B, Sreekanth P, Ramana Reddy MV, Philip R, Kalarikkal N (2015) Size dependent nonlinear optical absorption in $BaTiO_3$ nanoparticles. Chem Phys Lett 625:58–63
18. House WT, Orchin M (1960) A Study of the selenium dehydrogenation of guaiol and related compounds. Selenium as a hydrogen transfer agent. J Am Chem Soc 82:639–642
19. Rakshit T, Mondal SP, Manna I, Ray SK (2012) CdS-decorated ZnO nanorod heterostructures for improved hybrid photovoltaic devices. ACS Appl Mater Interfaces 4:6085–6095
20. Yuan K, Chen L, Chen YW (2014) Performance enhancement of bulk heterojunction solar cells with direct growth of CdS-cluster-decorated graphene nanosheets. Chem A Eur J 20:6010–6018
21. Chen D, Liu F, Wang C, Nakahara A, Russell TP (2011) Bulk heterojunction photovoltaic active layers via bilayer interdiffusion. Nano Lett 11:2071–2078
22. Cao AN, Liu Z, Chu SS, Wu MH, Ye ZM, Cai ZW, Chang YL, Wang SF, Gong QH, Liu YF (2010) A facile one-step method to produce grapheme-CdS quantum dot nanocomposites as promising optoelectronic materials. Adv Mater 22:103–106